PROGRESS IN PHOTOVOLTAICS: RESEARCH AND APPLICATIONS, VOL 2, 265-273 (1994)

Research

High-efficiency Silicon Solar Cells: Si/SiO_2 Interface Parameters and their Impact on Device Performance

A. G. Aberle,[1] S. W. Glunz,[2] A. W. Stephens,[1] and M. A. Green[1]

[1] *Centre for Photovoltaic Devices and Systems, University of New South Wales, P.O. Box 1, Kensington 2033, Australia;* [2] *Fraunhofer-Institut für Solare Energiesysteme (ISE), Oltmannsstrasse 22, 79100 Freiburg, Germany*

This article presents the first measurements of the parameters of the Si/SiO_2 interfaces employed on the record-efficiency silicon solar cells made at the University of New South Wales (UNSW). The UNSW oxides are characterized by very low values of the surface state density ($\sim 4 \times 10^9\ cm^{-2}\ eV^{-1}$), low values for the positive fixed oxide charge density ($\sim 7 \times 10^{10}\ cm^{-2}$) and a pronounced asymmetry in the capture cross-sections of electrons and holes. Using the microwave-detected photoconductance decay method, we verify experimentally that these oxide parameters produce a strong dependence of the effective surface recombination velocity at oxidized p-type silicon surfaces on the excess electron concentration within the wafer. In high-performance silicon solar cells, this phenomenon produces a long-wavelength spectral response that strongly depends on the bias light intensity, a characteristic 'hump' in the dark current–voltage characteristics and fill factors that are lower than would be expected from the high open-circuit voltages of 700 mV.

INTRODUCTION

Over the last decade, the energy conversion efficiency of terrestrial 1-sun silicon solar cells has been markedly increased from about 17% to more than 23%.[1] These achievements were mainly due to improved bulk minority carrier lifetimes and surface passivation properties. Surface recombination losses were reduced by new metallization schemes with minimized metallization fractions, by the optimization of the doping profiles below metallized and non-metallized surfaces and by passivating the non-metallized surfaces with a high-quality thermal oxide. Figure 1 shows a schematic representation of the PERL ('passivated emitter and rear locally diffused') cell. This cell design has been developed recently at the University of New South Wales (UNSW) and presently demonstrates the highest Air Mass 1.5 (AM1.5) efficiency (23.5%) of any silicon-based solar cell.[1,2]

In spite of the progress in the field of SiO_2-passivated silicon surfaces, recent research on PERL solar cells has revealed that recombination at the front and rear oxidized surfaces still contributes significantly to the total losses within the device.[3,4] This situation provides the motivation for the present paper, which serves two major purposes; first, it presents the first measurements of the parameters of the Si/SiO_2 interfaces employed on the UNSW high-efficiency silicon solar cells; second, it presents a review of the most important consequences of the Si/SiO_2 interface parameters on the electrical performance of the devices.

CCC 1062-7995/94/040265-9

Received 26 January 1994
Revised 1 March 1994

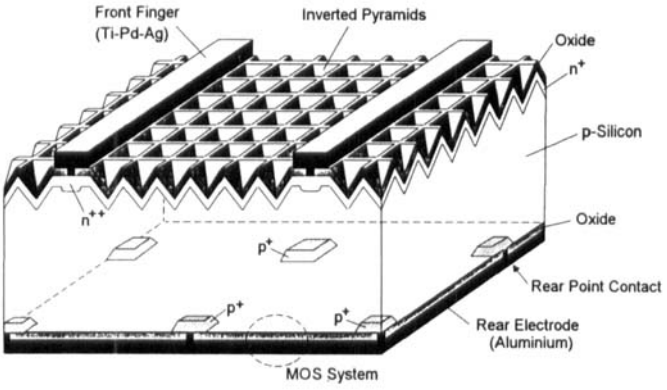

Figure 1. Schematic representation of the PERL silicon solar cell developed at the UNSW

SiO_2-PASSIVATED SILICON SURFACES

Processing sequence

The processing sequence for state-of-the-art thermally grown oxides as used on high-efficiency silicon solar cells is summarized in Table I.[5–7] The main steps are a dry thermal oxidation at high temperatures ($\sim$1000°C, with the possibility of up to 2% trichloroethane (TCA) being added to the oxygen), a post-oxidation anneal in an inert atmosphere (nitrogen or, preferably, argon) and a post-metallization anneal in forming gas. Trichloroethane is widely used in the photovoltaic community in order to ensure a high degree of cleanliness in the furnaces. Although TCA has not been found to be beneficial for the ultraviolet stability of point-contact silicon concentrator solar cells,[8] TCA is widely used in the fabrication of bifacially contacted 1-sun high-efficiency cells,[6,9] where no such stability problems have been observed. The oxidation time is very often chosen in order to produce about 105-nm thick oxides, so that the SiO_2 film also acts as a rudimentary antireflection coating on textured surfaces.

Si/SiO_2 interface parameters

In order to determine the oxide charge density Q_f and the dependence of the surface state density D_{it} and the capture cross-sections of electrons and holes (σ_n, σ_p) on the energy level of the surface state, metal-oxide semiconductor (MOS) capacitors (with aluminium gate electrodes) have been fabricated at UNSW using the processing sequence of Table I. These MOS capacitors were analysed at the Fraunhofer-Institut für Solare Energiesysteme (ISE) by means of a sensitive small-pulse 'deep-level transient spectroscopy' (DLTS) system and by low- and high-frequency capacitance–voltage ($C - V$) measurements.[7] The DLTS measurements showed very low surface state densities ($D_{it} \approx 4 \times 10^9$ cm^{-2} eV^{-1} at midgap) that were independent of the doping type of the silicon. These values are among the lowest ever reported surface state densities at thermally oxidized silicon surfaces. The energy dependence of D_{it} is similar to the U-shape measured for the high-quality Si/SiO_2 interfaces fabricated in the clean-room environment of the ISE.[7] Furthermore, as expected from the low D_{it} values,[10] the $C - V$ measurements revealed that the fixed oxide charge density Q_f is also very small. Table II summarizes the results obtained from the investigation of n- and p-type MOS capacitors.

In addition to the surface state density and the oxide charge density, the energy dependence of the capture cross-sections of electrons and holes has been determined from MOS-DLTS measurements. The results are plotted in Figure 2. These measurements are consistent with previously published experimental data,[7,11] indicating that the electron capture cross-section of most surface states is much larger than the capture cross-section of holes. Near midgap, the measured σ_n/σ_p ratio of the UNSW oxides is about

Table I. Processing sequence for the state-of-the-art thermal oxidation of high-efficiency silicon solar cells

Processing step	Details
Furnace cleaning	TCA, 1100°C
Wager cleaning	RCA clean
Wafer loading	$T \leqslant 800$°C, dry O_2
Heating	$\leqslant 10$°C min^{-1}
Oxidation	1050°C, dry O_2 ($\leqslant 2\%$ TCA optional)
Post-oxidation anneal	Ar, 15–30 min, 1050°C
Cooling	Ar, $\leqslant 10$°C min^{-1}
Unloading	$T \leqslant 800$°C
Post-metallization anneal	Forming gas (4% H_2), 400°C, 30 min)

Table II. Measured values of the surface state density D_{it} and the fixed oxide charge density Q_f on MOS capacitors fabricated at the UNSW (aluminium gate, 1-Ω·cm substrate, oxide thickness 105 nm)

	D_{it} at midgap (10^9 cm^{-2} eV^{-1})	Q_f (10^{10} cm^{-2})
p-Si	3–4	+6
n-Si	4–5	+8

50–70. As will be discussed in the following sections, PERL-type silicon solar cells take advantage of the relatively low hole capture cross-sections.

Effective surface recombination velocity at oxidized silicon surfaces

The strong asymmetry in the capture cross-sections of electrons and holes shown in Figure 2 produces a significant dependence of the effective surface recombination velocity S_{eff} at thermally oxidized p-type silicon surfaces on the excess minority carrier concentration within the wafer.[7,11–17] The best experimental techniques for revealing this dependence are measurements of the spectral response of rear-illuminated oxide-passivated bifacial silicon solar cells[7] and photoconductance decay (PCD) measurements[12,15,17] or modulated free-carrier absorption measurements[16] on oxidized silicon wafers. In all these methods the background excess minority carrier concentration within the wafer is adjusted using a bias light. As can be seen from Shockley–Read–Hall (SRH) recombination theory, the injection-level dependence of S_{eff} is fundamentally due to a transition from low to high injection conditions at the surface. Owing to the large σ_n/σ_p ratio, high injection effects occur first at the surface and then, with a significant delay, in the bulk itself. The effect is reinforced by the surface band bending induced by positive fixed oxide charges generally present at oxidized silicon surfaces.[3,4,7,14,18] At low injection levels in p-type wafers, the surface recombination process is limited by the availability of electrons at the surface, while at high injection levels the capture of holes represents the rate-limiting process.[3]

The theoretically expected behaviour is verified by the measurements of Figure 3, where S_{eff} at thermally oxidized non-metallized surfaces of p-type silicon wafers has been determined at UNSW by means of the microwave-detected photoconductance decay (MW-PCD) method.[15,17,19] The measurements show that, apart from very high injection levels, S_{eff} depends strongly on both the substrate resistivity and the excess electron concentration Δn in the substrate. Although the surface state density was found to be nearly independent of the substrate resistivity, S_{eff} increases strongly with reducing substrate resistivity. The low S_{eff} values at intermediate excess electron concentrations are due to the

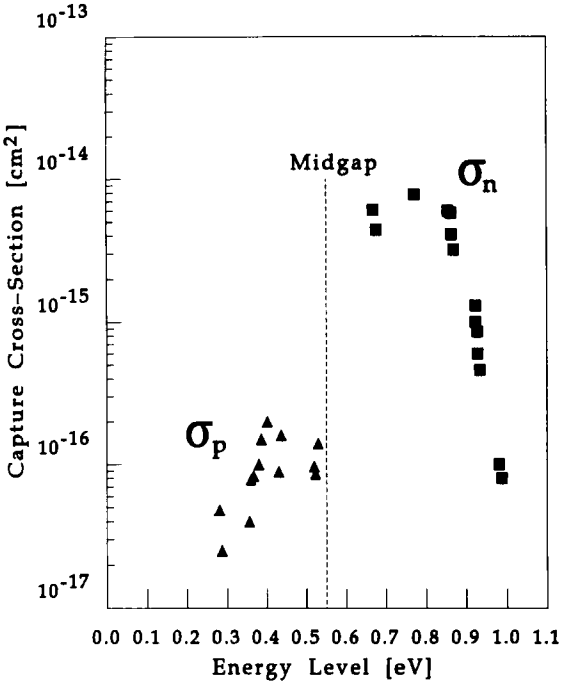

Figure 2. Measured energy dependence of the capture cross-sections of electrons and holes at thermally oxidized silicon surfaces processed at the UNSW (1 Ω·cm, oxide thickness 105 nm)

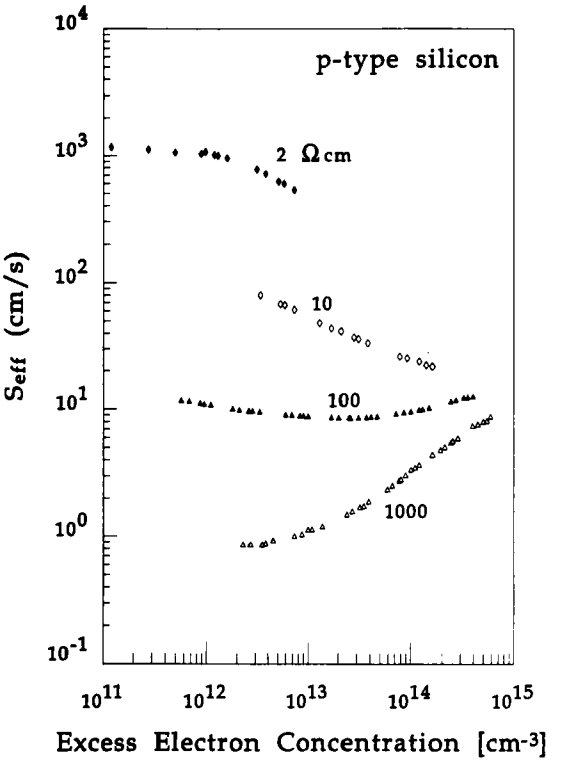

Figure 3. Measured dependence of the effective surface recombination velocity S_{eff} at thermally oxidized p-type silicon surfaces as a function of the substrate resistivity and the excess electron concentration within the wafer (oxide thickness 105 nm, oxides *not* covered by metal)

limited availability of holes at the oxidized surface ('depletion conditions'). With increasing excess electron concentration in the substrate the surface band bending reduces. Thus, the availability of holes at the surfaces increases, as does S_{eff}. Ultimately, at very high injection levels, the surface band bending becomes negligible and, owing to similar surface state densities, S_{eff} becomes independent of the substrate resistivity and the injection level.

For typical electron concentrations in the p-type base of 2-Ω·cm PERL cells (5×10^{12}–1×10^{16} cm^{-3} under 1-sun illumination), Figure 3 suggests S_{eff} values of 200–400 cm s^{-1} at the rear oxidized surface. However, special care has to be taken when comparing the S_{eff} values of PCD wafers with actual PERL-type solar cells. This is due to the fact that the rear oxide of the solar cell is covered by aluminium and thus forms a MOS system (see Figure 1). Coverage with Al has two important beneficial effects for S_{eff}. The first beneficial effect is that the 'hydrogen passivation effect' during the post-metallization forming gas anneal[14,20,21] is more pronounced compared to non-metallized oxidized surfaces. This is attributed to residual water in the SiO_2 film, which oxidizes aluminium and thereby produces higher concentrations of atomic hydrogen in the oxide compared to the standard forming gas anneal with bare oxidized wafers. The hydrogen atoms subsequently diffuse towards the Si/SiO_2 interface and passivate a significant fraction of the remaining surface states. The second beneficial effect of the coverage with Al is the surface band bending induced by work function differences in the Si–Al system.[3,7,18] On p-type silicon substrates, the work function of Al has an effect similar to an additional positive oxide charge. Thus, as a result of the coverage with Al, S_{eff} at the rear oxidized surface of PERL cells

is significantly smaller than is suggested by Figure 3. As will be shown in a later section, for 2-Ω·cm PERL cells the corresponding values lie in the 20–50 cm s^{-1} range near the 1-sun maximum power point.

IMPACT OF OXIDE PARAMETERS ON DEVICE PERFORMANCE

Spectral response

Figure 4 shows the measured external spectral response of a 280-μm thick 2-Ω·cm UNSW PERL solar cell with a planar (i.e. non-textured) front surface. These measurements were performed under short-circuit conditions and a variable amount of 'white' bias light. The relatively low spectral response values ($\leqslant 86\%$) are due to the large reflection losses associated with the 105-nm thick SiO_2 film on the planar front surface. According to Figure 4, the long-wavelength response of the cell improves strongly with increasing bias light intensity. For example, at 1000 nm, the use of bias light improves the measured spectral response by almost a factor of two. The reason for this behaviour is the injection-level dependence of S_{eff} at the rear surface, as indicated in Figure 3. Clearly, for accurate spectral response measurements of PERL-type silicon solar cells the use of bias light is mandatory.

Interestingly, the bias light has no effect on the blue response of the cell, indicating that the recombination velocity at the front oxidized surface is independent of the bias light level. This behaviour is attributed to the relatively high doping level ($\sim 5 \times 10^{18}$ cm^{-3}) at the front surface, ensuring that the front surface operates at low injection conditions under 1-sun illumination, independently from the cell bias. From both the excellent internal blue response and the high open-circuit voltages (~ 700 mV) of experimental PERL cells, we conclude that S_{eff} at the front oxidized surface is smaller than about 5000 cm s^{-1}.

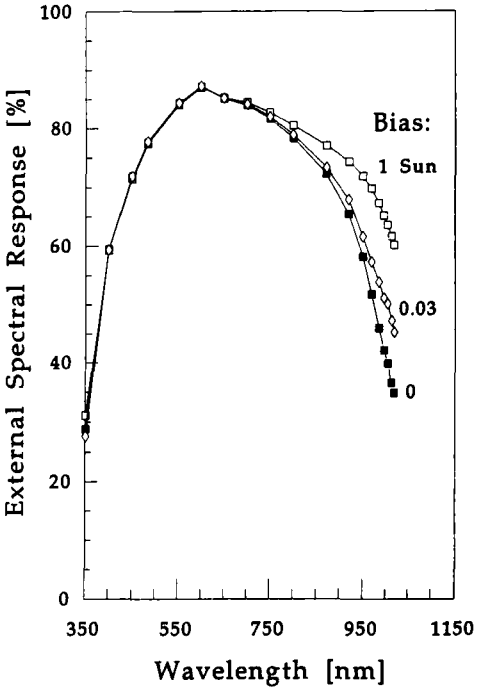

Figure 4. Measured external spectral response of a 280-μm thick 2-Ω·cm n^+p PERL-type silicon solar cell with planar front surface as a function of the bias light intensity (white bias light, measurements performed at short-circuit conditions, front oxide 105 nm, rear oxide 350 nm)

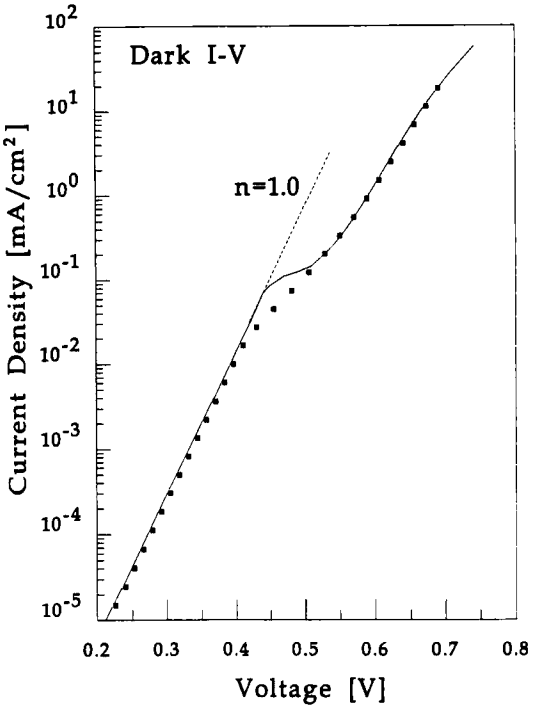

Figure 5. Measured dark I–V curve (squares) of a 280-μm thick 2-Ω·cm n^+p PERL-type silicon solar cell with planar front surface. The solid line is obtained from a two-dimensional simulation of the cell using measured oxide parameters

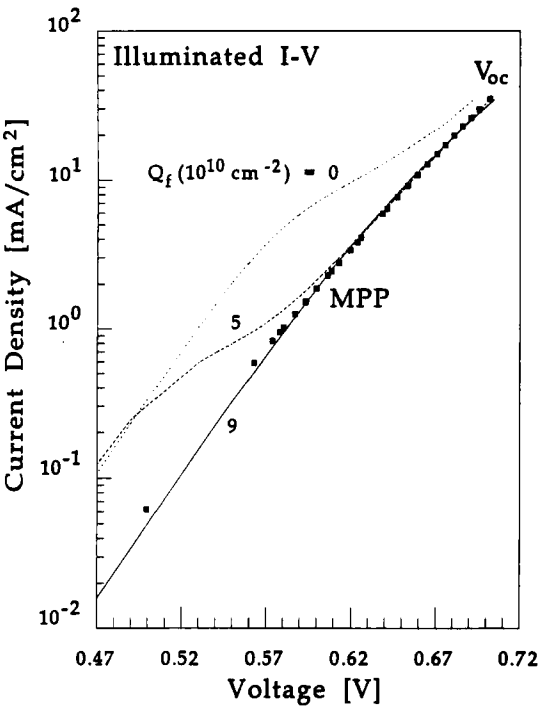

Figure 6. Comparison of theoretical (lines) and measured (squares) illuminated (AM1.5) I–V curves of a 280-μm thick 2-Ω·cm n^+p PERL-type silicon solar cell with planar front surface. MPP = maximum power point

Dark I–V curve

The dark squares in Figure 5 show the measured dark I–V characteristics of the above-mentioned PERL cell at room temperature. At low voltages, the cell exhibits the ideal diode behaviour with an ideality factor of unity. At intermediate voltages, however, the I–V curve starts to bend to the right (producing a characteristic 'hump') until a second straight-line segment (with an ideality factor higher than unity) is approached. The solid line in Figure 5, which fits the measured I–V curve very well, is obtained from a two-dimensional (2D) simulation of the cell.[4] The theoretical curve includes the band bending effects at the rear oxidized surface, the measured asymmetry of the electron and hole capture cross-sections and the effect of work function differences in the Al/p-Si system (which in the present cell is equivalent to an additional oxide charge density of $\sim 3 \times 10^{10}$ cm^{-2}). The less-than-ideal agreement between theory and experiment near the hump is attributed to the quasi-continuum of surface states in the real device; this creates a smoother transition compared to the modelled curve, which assumes a single surface state at midgap.

Illuminated I–V curve

Figure 6 shows a comparison of the measured illuminated 1-sun I–V curve (squares) with the theoretical predictions (lines) obtained from a 2D simulation of the cell.[4] For this plot the I–V curves were shifted by the short-circuit current density J_{sc} from the fourth quadrant (where they were originally measured) into the first quadrant. This method is well suited to investigate in detail the shape of the I–V curve

between the maximum power point and the open-circuit voltage. Owing to light intensity fluctuations, the experimental data are limited to current densities greater than 0.05 mA cm^{-2}.

The solid line, which fits the experimental $I-V$ curve very well, was obtained from a 2D simulation of the device using the measured oxide parameters of the earlier section on Si/SiO_2 interface parameters (in order to include the Al work function effect, an additional oxide charge density of $\sim 3 \times 10^{10}$ cm^{-2} was added to the measured value of Table II). The two additional dashed lines are 2D results revealing the enormous impact of positive oxide charges on the $I-V$ curve of PERL cells. Clearly, with increasing oxide charge density Q_f, the efficiency of the solar cell improves. This behaviour has initiated research efforts at UNSW aiming at increased Q_f values at the Si/SiO_2 interface without deterioration of the surface state density D_{it}. The 2D simulations also show that S_{eff} at the rear oxidized surface of 2-$\Omega \cdot$cm PERL cells is about 20–50 cm s^{-1} near the 1-sun maximum power point. Although these values are one order of magnitude lower than the corresponding S_{eff} values of 2 $\Omega \cdot$cm bare-oxide wafers measured by the MW-PCD method (see Figure 3), recombination losses at the rear oxidized surface of PERL cells contribute about 25% to the total losses at the 1-sun maximum power point, while a similar contribution comes from the front oxidized surface.[4]

In spite of the exceptionally high open-circuit voltages of about 700 mV, PERL cells have demonstrated relatively modest fill factors below 81%, compared to earlier generations of UNSW cells that have demonstrated fill factors in the 83–84% range. From an analysis of measured illuminated $I-V$ curves of PERL cells we conclude that the low fill factors are due to the injection-level-dependent surface recombination velocity at the rear oxidized surface, to less-than-ideal values for the series resistance R_s (typically 0.3–0.4 $\Omega \cdot cm^2$ at the 1-sun maximum power point) and onset of high-injection conditions in the base towards open-circuit conditions, leading to a higher than unity ideality factor near V_{oc}. The 2D simulations furthermore show that the cell efficiency can be improved by the use of thicker substrates; this helps the short-circuit current and reduces the detrimental impact of the injection-level-dependent S_{eff} at the rear oxidized surface on the fill factor. By using considerably thicker wafers (400 μm compared to the 250–280 μm of earlier PERL cells), we were able to realize experimentally PERL cell fill factors as high as 82.7% and record efficiencies of 23.5% on textured 1-$\Omega \cdot$cm substrates.[2] A detailed discussion of the efficiency-limiting mechanisms in 23% efficient PERL cells is beyond the scope of this paper and will be presented elsewhere.[22]

SUMMARY

Recombination losses at the oxidized front and rear surfaces play an important role in limiting the performance of present high-efficiency PERL silicon solar cells made at the UNSW. This work presents the first measurements of the parameters of the Si/SiO_2 interfaces employed on these devices. The UNSW oxides are characterized by very low values of the surface state density ($\sim 4 \times 10^9$ cm^{-2} eV^{-1}), low values for the positive fixed oxide charge density ($\sim 7 \times 10^{10}$ cm^{-2}) and a pronounced asymmetry in the capture cross-sections of electrons and holes ($\sigma_n/\sigma_p = 50$–70 near midgap).

Using the MW-PCD method, we have verified that these oxide parameters produce a strong dependence of the effective surface recombination velocity S_{eff} at oxidized p-type silicon surfaces on the excess electron concentration within the wafer. In experimental PERL cells, this phenomenon produces a long-wavelength spectral response that depends strongly on the intensity of the bias light, a characteristic hump in the dark current–voltage characteristics and fill factors that are lower than would be expected from the high open-circuit voltages of 700 mV.

By increasing the wafer thickness, the impact of the injection-level-dependent rear surface recombination velocity on the device performance can be reduced. On 400-μm thick substrates we have achieved fill factors of up to 82.7% and cell efficiencies of up to 23.5%. Furthermore, research efforts have commenced aiming at an increased oxide charge density Q_f without deterioration of the surface state density D_{it}.

Acknowledgements

The Centre for Photovoltaic Devices and Systems is supported by the Australian Research Council's Special Research Centres Scheme and Pacific Power. We would like to thank Aihua Wang and Jianhua Zhao from the Photovoltaic Centre for processing the investigated devices and Wilhelm Warta from Fraunhofer-Institut für Solare Energiesysteme for the spectral response measurements. One of the authors (A.G.A.) gratefully acknowledges the support of a Feodor Lynen Fellowship provided by the German Alexander von Humboldt Foundation. A.W.S. gratefully acknowledges the financial support of an Australian Postgraduate Research Award and a University of New South Wales Supplementary Engineering Scholarship.

REFERENCES

1. M. A. Green and K. Emery, 'Solar cell efficiency tables' (version 4), *Progr. Photovolt*, **2**, 231–234 (1994).
2. J. Zhao, A. Wang and M. A. Green, '23.5% efficient silicon solar cells', *Progr. Photovolt.*, **2**, 227–230 (1994).
3. A. G. Aberle, S. J. Robinson, A. Wang, J. Zhao, S. R. Wenham and M. A. Green, 'High-efficiency silicon solar cells: fill factor limitations and non-ideal diode behaviour due to voltage-dependent rear surface recombination velocity', *Progr. Photovolt*, **1**, 133 (1993).
4. A. G. Aberle, G. Heiser and M. A. Green, 'Two-dimensional numerical optimisation study of the rear point-contact geometry of high-efficiency silicon solar cells', *J. Appl. Phys.* (May 1994).
5. R. A. Sinton, Y. Kwark, S. Swirhun and R. M. Swanson, 'Silicon point contact concentrator solar cells', *IEEE Trans. on Devices Lett.*, **6**, 405 (1985).
6. A. W. Blakers, A. Wang, A. M. Milne, J. Zhao and M. A. Green, '22.8% Efficient silicon solar cell', *Appl. Phys. Lett.*, **55**, 1363 (1989).
7. A. G. Aberle, S. Glunz and W. Warta, 'Impact of illumination level and oxide parameters on Shockley–Read–Hall recombination at the Si–SiO_2 interface', *J. Appl. Phys.*, **71**, 4422 (1992).
8. P. E. Gruenbaum, J. Y. Gan, R. R. King and R. M. Swanson, 'Stable passivations for high-efficiency silicon solar cells', *Conf. Rec. 21st IEEE Photovoltaic Specialists Conference*, Kissimmee, USA, p. 317.
9. J. Knobloch, A. Noel, E. Schäffer, U. Schubert, F. J. Kamerewerd, S. Klussman and W. Wettling, 'High-efficiency solar cells from FZ, CZ and MC silicon material', *Conf. Rec. 23rd IEEE Photovoltaic Specialists Conference*, Louisville, USA, 1993, p. 271.
10. R. R. Razouk and B. E. Deal, 'Dependence of interface state density on silicon thermal oxidation process variables', *J. Electron. Soc.*, **126**, 1573 (1979).
11. W. D. Eades and R. M. Swanson, 'Calculation of surface generation and recombination velocities at the Si–SiO_2 interface', *J. Appl. Phys.*, **58**, 4267 (1985).
12. R. R. King, R. A. Sinton and R. M. Swanson, 'Low surface recombination velocities on doped silicon and their implications for point contact solar cells', *Conf. Rec. 19th IEEE Photovoltaic Specialists Conference*, New Orleans, USA, 1987, p. 1168.
13. J. Knobloch, A. G. Aberle, W. Warta and B. Voss, 'Dependence of surface recombination velocities at silicon solar cell surfaces on incident light intensity', *Conf. Rec. 8th European Communities Photovoltaic Solar Energy Conference*, Florence, Italy, 1988, p. 1165.
14. A. G. Aberle, S. Glunz, W. Warta, J. Kopp and J. Knobloch, 'SiO_2-passivated high efficiency silicon solar cells: process dependence of Si–SiO_2 interface recombination', *Conf. Rec. 10th European Communities Photovoltaic Solar Energy Conference*, Lisbon, Portugal, 1991, p. 631.
15. T. Uematsu, Y. Nagata, T. Ohtsuka, T. Warabisako, H. Nomura, T. Iga and T. Saitoh, 'Degradation free SiO_2 passivation layer oxidized by TCA process', *Conf. Rec. 23rd IEEE Photovoltaic Specialists Conference*, Louisville, USA, 1993, p. 352.
16. S. W. Glunz, A. B. Sproul, W. Warta and W. Wettling, 'Injection level dependent recombination velocities at the Si–SiO_2 interface for various dopant concentrations', *J. Appl. Phys.*, **75**, 1611 (1994).
17. A. W. Stephens, A. G. Aberle and M. A. Green, 'Surface recombination velocity measurements at the silicon–silicon dioxide interface by microwave-detected photoconductance decay', *J. Appl. Phys.* (May 1994).
18. A. G. Aberle, S. Glunz and W. Warta, 'Field effect passivation of high efficiency silicon solar cells', *Sol. Energy Mater. Sol. Cells*, **29**, 175 (1993).

19. P. A. Basore and B. R. Hansen, 'Microwave-detected photoconductance decay', *Conf. Rec. 21st IEEE Photovoltaic Specialists Conference*, Kissimmee,USA, 1990, p. 374.
20. B. E. Deal, E. L. MacKenna and P. L. Castro, 'Characteristics of fast surface states associated with SiO_2–Si and Si_3N_4–SiO_2–Si structures', *J. Electrochem. Soc.*, **116**, 997 (1969).
21. E. H. Nicollian and J. R. Brews, *MOS (Metal Oxide Semiconductor) Physics and Technology*, Wiley, New York, 1982.
22. A. G. Aberle, P. Altermatt, G. Heiser, S. J. Robinson and M. A. Green, 'Limiting loss mechanisms in 23% efficient silicon solar cells', submitted to *J. Appl. Phys.* (1994).